Author/s:
Brown, WGA;Needham, K;Begeng, JM;Thompson, AC;Nayagam, BA;Kameneva, T;Stoddart, PR

Title:
Thermal damage threshold of neurons during infrared stimulation

Date:
2020-04-01

Citation:
Brown, W. G. A., Needham, K., Begeng, J. M., Thompson, A. C., Nayagam, B. A., Kameneva, T. & Stoddart, P. R. (2020). Thermal damage threshold of neurons during infrared stimulation. Biomedical Optics Express, 11 (4), pp.2224-2234. https://doi.org/10.1364/BOE.383165.

Persistent Link:
https://hdl.handle.net/11343/237413

Research Article | Vol. 11, No. 4 / 1 April 2020 / Biomedical Optics Express 2224
Biomedical Optics EXPRESS

Thermal damage threshold of neurons during infrared stimulation

WILLIAM G. A. BROWN,[1] KARINA NEEDHAM,[2] JAMES M. BEGENG,[1] ALEXANDER C. THOMPSON,[3] BRYONY A. NAYAGAM,[4] TATIANA KAMENEVA,[1] AND PAUL R. STODDART[1,*]

[1]*Faculty of Science, Engineering and Technology, Swinburne University of Technology, John Street, Hawthorn, VIC 3122, Australia*
[2]*Department of Surgery (Otolaryngology), University of Melbourne, Royal Victoria Eye & Ear Hospital, 32 Gisborne St, East Melbourne, VIC 3002, Australia*
[3]*The Bionics Institute, East Melbourne, VIC 3002, Australia*
[4]*Department of Audiology and Speech Pathology, University of Melbourne, Parkville, VIC 3010, Australia*
[*]*pstoddart@swin.edu.au*

Abstract: In infrared neural stimulation (INS), laser-evoked thermal transients are used to generate small depolarising currents in neurons. The laser exposure poses a moderate risk of thermal damage to the target neuron. Indeed, exogenous methods of neural stimulation often place the target neurons under stressful non-physiological conditions, which can hinder ordinary neuronal function and hasten cell death. Therefore, quantifying the exposure-dependent probability of neuronal damage is essential for identifying safe operating limits of INS and other interventions for therapeutic and prosthetic use. Using patch-clamp recordings in isolated spiral ganglion neurons, we describe a method for determining the dose-dependent damage probabilities of individual neurons in response to both acute and cumulative infrared exposure parameters based on changes in injection current. The results identify a local thermal damage threshold at approximately 60 °C, which is in keeping with previous literature and supports the claim that damage during INS is a purely thermal phenomenon. In principle this method can be applied to any potentially injurious stimuli, allowing for the calculation of a wide range of dose-dependent neural damage probabilities. Unlike histological analyses, the technique is well-suited to quantifying gradual neuronal damage, and critical threshold behaviour is not required.

1. Introduction

Artificial stimulation of neurons constitutes the backbone of investigative electrophysiology and translational neuroscience. Whilst direct-contact electrical stimulation remains the gold standard in neural prosthesis design, novel stimulation methods such as optogenetics, infrared stimulation, acoustic stimulation and magnetic stimulation have the potential to be less invasive, whilst offering improved spatial and temporal resolution [1,2]. Evaluating the safe operating parameters of these techniques is essential for their clinical translation, and typically relies on histological analysis of the target cells or fluorescence staining using dye assays *ex situ*. These detection methods are usually destructive, making them unsuitable for observing the time course of neural degradation.

Where the experimental regime permits, an *in situ* non-destructive indicator of neural damage is often more desirable. Patch-clamp techniques for intracellular electrophysiological recording can provide real-time measurements of a neuron's membrane potential, impedance and transmembrane current. Membrane impedance decreases as a damaged cell membrane becomes more permeable, and has previously been demonstrated as a useful measurement of induced

#383165 https://doi.org/10.1364/BOE.383165
Journal © 2020 Received 22 Nov 2019; revised 11 Feb 2020; accepted 23 Mar 2020; published 27 Mar 2020

Biomedical Optics EXPRESS

cell damage [3]. With proper statistical treatment, membrane impedance can provide a useful estimate of stimulus-dependent damage probability over the course of an experiment.

Pulsed infrared light is capable of modulating firing in a wide range of neurons [4–14]. Localised absorption of light by water molecules has been shown to evoke small thermal transients in neural tissue, [5,6] capable of driving membrane depolarisation through a combination of optocapacitive and ion channel-modulating mechanisms [6,7,15]. The associated risk of thermal damage using this technique has previously been characterised by histological analysis in rat sciatic nerves [16], rodent and primate cerebral cortices [17], rat astrocytes [18] and multiple mammalian cochlear models [8,19–22], which have demonstrated significant variation by tissue type and pulse repetition rate.

We monitored changes in the membrane impedance of spiral ganglion neurons (SGNs) stimulated by 1870 nm pulsed infrared light, and calculated the probability of cell damage for four exposure parameters. A multi-target single-hit (MTSH) model was used to describe rapid-onset damage, which was dependent on single-recording (acute) parameters, whilst cumulative exposure damage was quantified by a Weibull distribution. The results support an assertion that neural damage during infrared stimulation is a purely thermal phenomenon, and identify a sharp increase in damage probability above 60 °C, which is broadly in agreement with previous histological analyses. The methodology presented in this study is not limited to quantifying thermal damage, and can in principle be used to calculate dose-dependent neural damage thresholds for a wide range of exogenous stimuli.

2. Methods

2.1. Experimental setup

The method used for infrared stimulation and patch clamp recording has been described elsewhere [23]. Briefly, spiral ganglion neurons (SGNs) were dissociated from postnatal 4-7 day old Wistar rat pups, using a combination of enzymatic (0.025% trypsin and 0.001% DNase I) and mechanical techniques. Cells were suspended in Neurobasal medium (by volume: 95% Neurobasal A, 1% N2 supplement, 2% B27 supplement, 1% L-glutamine, 1% penicillin-streptomycin) cultured at 37 °C with 10% CO2, and replaced with fresh medium four hours after plating and subsequently every 24-48 hours. Neurotrophins (BDNF and NT-3) were added at a concentration of 10-50 ng mL^{-1}. Experiments were conducted on cells after 1-3 days in culture. All protocols were approved by the Animal Research and Ethics Committee of the Royal Victorian Eye and Ear Hospital in Melbourne, Australia.

Borosilicate micropipettes (2-6 MΩ) were prepared using a CO2 laser puller (P-2000; Sutter instruments) and filled with intracellular solution (115 mM K-gluconate, 7 mM KCl, 10 mM HEPES, 0.05 mM EGTA, 2 mM Na2ATP, 2 mM MgATP, 0.5 mM Na2GTP). Cell cultures were immersed in extracellular solution (137 mM NaCl, 5 mM KCl, 2 mM CaCl2, 1 mM MgCl2, 10 mM HEPES, 10 mM glucose) for recording, with a perfusion rate of 1-2 ml/min. The return electrode for the patch clamp circuit was placed in the extracellular bath 10-20 mm from the target cell.

To investigate the role of ambient temperature, the extracellular solution was either kept at room temperature (22.4±2.2 °C, N=78 neurons), or elevated to 30.4±3.4 °C (N=15) using an inline heater (SH-27B, Warner Instruments). Infrared illumination from an 1870 nm laser diode (Renoir, Aculight Corp.) was delivered through a 200/220 μm diameter fibre (NA=0.22) positioned proximally to the cell. An illustration of the recording and illumination setup is provided in Fig. 1.

The laser spot size can be calculated directly from the fibre geometry [23], but was not done for this study. Thompson et al. previously found that for an aqueous-submerged fibre tip, absorption of light across the entire beam path complicates the relationship between irradiance and infrared-evoked heating in tissue [24]; consequently the laser pulses have been parameterised

Biomedical Optics EXPRESS

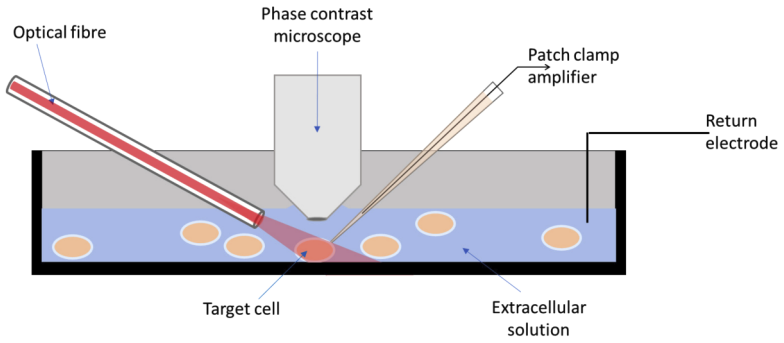

Fig. 1. Experimental setup. SGN cultures were immersed in extracellular solution, and healthy cells were located through a phase contrast microscope (not to scale). Infrared light was delivered through an optical fibre attached to a micromanipulator, and electrophysiological recordings were obtained through a patch-clamping electrode attached to an amplifier.

here in terms of energy per pulse and peak laser power. The position of the fibre relative to the SGN was replicated between recordings by observing the position of the upper edge of the optical fibre through the objective, and keeping this distance constant for each recording. The magnitude of the evoked temperature increase was determined experimentally using the method described below.

2.2. Stimulation and recording

The transmembrane current was recorded from a sample of 93 neurons under various voltage-clamp protocols. All neurons were first clamped at -73 mV holding potential and interrogated by a small (-10 mV, 20 ms) voltage pulse to record input resistance. After a one second delay, membrane potential was either maintained at -73 mV (fixed voltage protocol), or stepped across a pre-defined range of holding potentials (-103 mV to -23 mV or -73 mV to +27 mV) in +10 mV, 320 ms steps with a 150 ms return to -73 mV after each step (stepped-voltage protocol). For the fixed-voltage protocol, a train of 20 laser pulses was delivered at either 0.5, 1, 2, 4 or 10 Hz, which constituted one full recording. For the stepped-voltage protocol, one laser pulse was delivered for each holding potential value 130 ms after the beginning of each voltage step, and a single recording was defined as a full set of voltage steps. Differences between the voltage-clamp protocols were not observed to affect cell viability, and our results here are aggregated in terms of laser pulse parameters.

Figure 2 shows an example of a relatively rapid decline in cell health, as inferred from an increase in transmembrane current magnitude during a stimulation pulse sequence. Membrane resistance was calculated from changes in transmembrane current under the assumption of Ohmic resistance, which has previously been shown to be a good approximator of cell injury [3,25–27]. In particular, a decrease in membrane resistance has been correlated with conformational maladies in the membrane (e.g. blebbing and perforation) [3], which are commonly associated with thermal damage during INS [28–30]. Cells were classified as damaged when the input resistance decreased by 30% from the first recorded value, which was found to provide a good approximation for the point at which a qualitative deterioration in the quality of recordings was observed. However, this −30% cut-off can be modified to implement a more or less strict definition of cell damage as required.

From the sample of 93 neurons a total of 747 recordings were analysed, employing laser powers between 0.3–1.6 W and pulse durations of 0.2–5.0 ms. Both laser power and pulse duration were fixed for each recording, and are termed acute parameters. The additional acute parameters of

Biomedical Optics EXPRESS

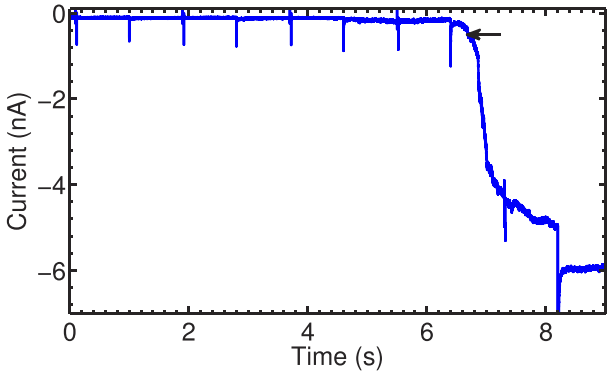

Fig. 2. A relatively rapid decline in cell viability. This rapid increase in injection current (indicated by the arrow) during a voltage clamp recording provided a clear indication of cell damage.

energy per pulse (peak power × pulse duration) and average power (∑ pulse energies / recording duration) were calculated from these values. During analysis, laser power was used as an indicator of the rate of laser-evoked temperature change (the temperature gradient), whilst energy per pulse and average power were taken as indicators of short-term (millisecond) and long-term (seconds) heating, respectively.

When the membrane current for a given recording satisfied the −30% damage threshold, damage was attributed to the most recently employed acute exposure parameters. To investigate the effects of infrared exposure over a cell's lifetime, the cumulative energy exposure (∑ pulse energies) of all pulses prior to cell death was tracked as a cumulative parameter. The different statistical treatment of acute and cumulative parameters is outlined below.

2.3. Statistical analysis

2.3.1. Histogram bin width

To establish the probability of cell damage for each parameter, histograms were constructed to show the number of recordings made across the tested parameter range. Initial histogram bins were determined by one of two methods: even division of the data range by the square root of the number of data points (bin size = range/$\sqrt{N}$), or the Freedman-Diaconis rule (bin size = 2 IQR $N^{-1/3}$, where IQR is the interquartile range). In the former case, bins which were not empty but contained less than 10% of the recordings were incrementally increased in width by 10% of their original size until they either contained ≥10% of the data points or had been increased in width five times. This was done to better optimise the number of recordings in each bin for the purpose of calculating damage probabilities. For each parameter, the selected method was chosen according to which one provided the most evenly distributed histogram across the entire data range.

The probability of cell damage (P_d) was calculated for each bin by dividing by the number of recordings ($P_d = N_{damaged}/N$), and binomial confidence intervals were calculated using the Wilson interval method [31], defined by:

$$\frac{1}{1+1/Nz^2}\left(P_d + \frac{1}{2N}z^2 \pm \sqrt{\frac{1}{N}P_d(1-P_d) + \frac{1}{4N^2}z^2}\right), \tag{1}$$

where $z = 1$ such that the confidence intervals correspond to one standard deviation.

Biomedical Optics EXPRESS

2.3.2. Multi-target single-hit model (acute parameters)

Acute parameters were fitted to a multi-target single-hit (MTSH) model, typically used to construct cell survival curves in response to ionising radiation [32]. Under this model, cell death is said to occur when a certain number of targets within the cell sustain damage. Targets are defined as non-specific cellular structures, and do not have direct analogues, making this a purely phenomenological model. The MTSH model defines a monotonically increasing acute damage probability $P_a(x)$:

$$P_a(x) = \left[1 - exp\left(\frac{-x}{x_0}\right)\right]^n \tag{2}$$

where n is the number of targets that must be damaged in order for a cell to perish, and $\frac{x}{x_0}$ is the average number of targets hit when a cell is exposed to dose x. $P_a(x)$ was fitted to the damage probability data P_d for each acute parameter x, from which values for x_0 and n could be extracted.

2.3.3. Weibull distribution (cumulative parameters)

Cell damage probabilities for cumulative parameters were fitted to the Weibull cumulative distribution function, a model for cumulative failure probability $P_c(x)$:

$$P_c(x) = 1 - exp\left[\left(\frac{-x}{\eta}\right)^{\nu}\right] \tag{3}$$

where x is the independent variable, η is the Weibull scale parameter and ν is the Weibull shape parameter. The value of ν is of particular interest as a descriptor of the change in failure rate with respect to quantity x, in this case the cumulative energy exposure. A value of $\nu<1$ indicates that the rate of failure decreases with increasing x, whilst $\nu=1$ and $\nu>1$ indicate constant and increasing failure rates respectively. In a similar manner to the MTSH model, values for η and ν were extracted from the best-fit expression for $P_c(x)$ to the damage probability data $P_d(x)$ for cumulative exposure. Note that although the form of the Weibull distribution resembles that of the MTSH model, its logical rationale is distinct.

2.4. Temperature calibration

Laser-evoked temperature changes were recorded using the open patch pipette method described by Yao et al.[33], which has become a common technique for measuring temperature rise during INS [6,18,29,34–36]. Briefly, a micropipette tip was placed in the extracellular bath at a known elevated temperature (typically 30–35 °C, as recorded via thermocouple) in a position representative of that used for patch-clamp recordings. The pipette resistance was then measured at regular intervals as the solution was allowed to cool to room temperature. Constructing an Arrhenius plot allowed us to relate the resistance to local temperature at the pipette tip. After this calibration was completed, laser-evoked temperature changes in the extracellular solution could be approximated directly from the change in pipette resistance. Initial temperature calibrations were assumed to be accurate if the Arrhenius plot was approximately linear, corresponding to a constant activation energy for the extracellular bath [33].

3. Results

3.1. Acute parameters

Acute damage probabilities were analysed on a per-recording basis with the goal of placing an upper limit on the tolerable short-term exposure parameters for SGNs. Cell damage probability P_d exhibited no dependence on peak laser power in both the room temperature (22.4 °C) and elevated temperature (30.4 °C) conditions, up to a maximum of 1.5 W (Fig. 3(a, b)). As discussed above, the open patch pipette method [33] was used to relate the laser pulse power to the heating

Biomedical Optics EXPRESS

rate, demonstrating a linear proportionality with a coefficient of 8.92 °C W^{-1} ms^{-1}. The fact that this temperature gradient was both linear (R^2=0.996) and tended to zero for small laser powers was taken to be a good indication of the accuracy of the temperature recordings (for small pulses), and used to calculate the maximum temperature gradient for each SGN. Our results suggest that SGNs can safely tolerate temperature gradients of at least 14 °C ms^{-1} during infrared exposure, and appears to rule out the possibility of cellular damage due to phototoxic interactions, which would be expected to scale with photon flux.

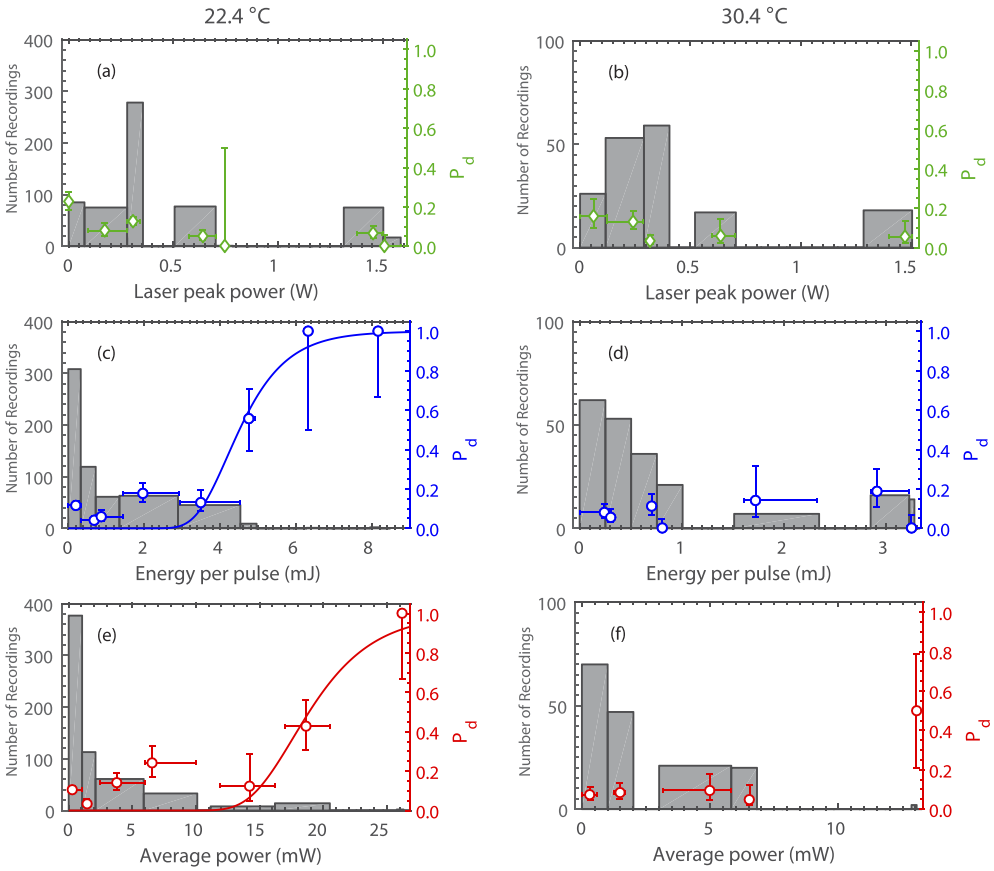

Fig. 3. Acute damage probabilities. Histograms (left axis) and corresponding damage probabilities (right axis) for the following illumination parameters: **(a, b)** laser peak power, **(c, d)** energy per pulse, and **(e, f)** average power. Data points represent damage probabilities with standard errors. Plots (a, c, e) are for room temperature recordings (22.4 °C) and plots (b, d, f) are for elevated (30.4 °C) temperature recordings. Solid lines are best-fit equations for the MTSH model.

In contrast, an increase in laser pulse energy was strongly correlated with higher cell damage probability at room temperature (Fig. 3(c)). A rapid increase in damage probability was observed at 4 mJ, increasing to 90% at approximately 6 mJ as calculated from best-fit MTSH model parameters (x_0 = 0.848 mJ, n = 140). No relationship with pulse energy was observed in the 30 °C condition (Fig. 3(d)), but it should be noted that none of the pulse energies analysed in the 30 °C data set exceeded the 4 mJ threshold at which P_d was observed to increase in the room-temperature condition. This was due to the initial data sets prioritising an investigation of laser-evoked depolarisations over that of neural damage probabilities: obtaining a stable neuronal

Biomedical Optics EXPRESS

recording was found to be more challenging in the elevated-temperature condition, so more conservative pulse energies were generally used to improve recording duration.

Higher average power values also resulted in an increase in cell damage probability at room temperature (Fig. 3(e)), but could not be verified for the 30 °C condition due to a lack of data above 15 mW (Fig. 3(f)). The probability of damage P_d was characterised by MTSH parameters x_0 = 3.45 mJ and n = 168, which predicted a 50% damage probability at 19 mW, and a 90% probability at 25 mW. The rapid increase to P_d = 0.5 at around 15 mW for the elevated temperature condition could be indicative of a reduced damage threshold for higher ambient temperatures, but cannot be relied upon due to a large standard deviation.

In almost all recordings, membrane resistance decreased monotonically over the duration of each recording. However, it is important to note that since cells were discarded shortly after the −30% damage threshold was satisfied, we cannot rule out the possibility that membrane resistance could be restored if allowed a sufficiently long recovery period. Although recovery was not observed on our short experimental timescales, there is some limited evidence to suggest that laser-induced membrane poration is sometimes a reversible process [30,37]. Some resistance fluctuations may also have been due to laser-evoked pressure waves loosening the patching seal, but it is unclear whether a loosened seal could recover if given sufficient time. Therefore we identify the potential for long-term recovery of the membrane resistance following laser exposure as an area of future study.

3.2. Cumulative energy exposure

The damage probability increased monotonically with respect to total energy exposure, but exhibited a diminishing rate of increase at higher exposures, as shown in Fig. 4(a). This relationship was well characterised by a Weibull shape parameter of less than one (ν = 0.595, η = 692). This may be indicative of a survivorship bias whereby cells that survive beyond a certain level of exposure (approx. 300 mJ) are more robust, whilst more fragile cells are eliminated relatively early in the stimulation protocol. The fitted distribution predicted a 50% damage probability at around 400 mJ total exposure.

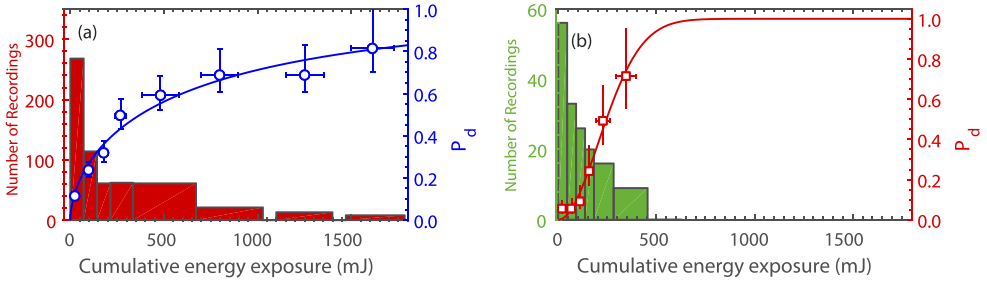

Fig. 4. Damage probability due to cumulative energy exposure. Histograms (left axis) and corresponding damage probabilities (right axis) for cumulative energy exposures at ambient extracellular temperatures of **(a)** 22.4°C and **(b)** 30.4°C. Data points represent damage probabilities with standard errors, and solid lines are best-fit Weibull distribution models for each data set.

By contrast, at 30 °C the Weibull shape parameter for the damage probability due to total energy exposure was greater than one (ν=1.95, η=296), indicating an increase in the rate of failure at higher total exposures (Fig. 4(b)). Notably, this distribution predicts a 100% damage probability at cumulative exposures above about 500 mJ, and a 50% damage probability at 250 mJ. However, no data was collected for cells with greater than 500 mJ exposure at 30 °C, which limits the reliability of predictions in this range.

Biomedical Optics EXPRESS

The apparent shift of the fitted Weibull distribution curve to lower energies for the 30 °C condition suggests that at room temperature, SGNs are more robust to the cumulative effects of infrared illumination than cells in the elevated temperature condition. In the context of our acute damage results, this seemed to indicate the presence of an absolute temperature threshold as the primary mode of cell failure. To investigate this further, we calculated the maximum temperature reached for each recording of acute cell failure, and calculated P_d with respect to peak temperature in a MTSH model.

3.3. Thermal threshold

The maximum temperature change $\Delta T_{\max}$ evoked by a single laser pulse was estimated using the open patch pipette method. To calculate $\Delta T_{\max}$ for a single pulse, the previously calculated temperature gradient coefficient $dT/dt = 8.92\ °C\ W^{-1}\ ms^{-1}$ (see *acute parameters*) was multiplied by the pulse-specific laser power and pulse duration. To calculate $\Delta T_{\max}$ for an entire pulse train recording, inter-pulse cooling was approximated using the two-term exponential decay expression reported by Thompson et al.[38]. The peak temperature achieved during a recording was the sum of $\Delta T_{\max}$ at the end of the pulse train and the ambient temperature of the cell bath (either 22.4 °C or 30.4 °C).

Figure 5 shows the probability of cell damage as a function of peak temperature, which was treated as an acute parameter. The room-temperature MTSH model ($x_0 = 4.44$ and $n = 1.83\times10^6$) possesses a broadly similar shape to those of energy per pulse and average power, and identifies a threshold-like behaviour of P_d above 60 °C ($P_d = 0.1$ at 60.3 °C). Importantly, the data does not provide any evidence that the initial temperature had any effect on the relationship between damage probability and peak temperature, although more data points are required for the 30.4 °C condition to confirm an absence of dependency. Straightforward calculations from this model estimate a 20% damage probability at 62.0 °C, a 50% probability at 65.7 °C, and a 90% probability at 74.0 °C. Therefore the width of the threshold region is similar to the temperature difference for cells at 22.4 °C and 30.4 °C. However, note that this model does not take heat flow effects into account, and may thus have a tendency to overestimate the temperature change for longer pulses.

The thresholds summarised above are broadly in keeping with the peak temperature changes reported by several previous histological studies [5,16,18]. However, for hyperthermic injury both the magnitude of the temperature increase and the duration of exposure must be taken into account [40]. Consequently, data from studies conducted on different timescales has limited usefulness when used for direct comparison. However, a study conducted on *in vitro* renal carcinoma cells by He and Bischof [39] utilised timescales only one order of magnitude slower than our own (up to 130 °C min^{-1}), and provides remarkably good agreement with our data.

The fact that an order of magnitude difference in heating rates would have such a small effect on damage probability may indicate the presence of a thermal damage threshold at which damage occurs rapidly enough that differences in heating duration are relatively insignificant. The damage probability predicted by our thermal MTSH model increased from 0.2 to 0.9 over the span of 12 °C, which is a similar temperature range to the protein denaturation transition width [28]. Whilst it should be noted that this similarity may be coincidental, protein denaturation has previously been implicated in hyperthermic cell injury [28,40]. With this in mind, it seems feasible that the sharp thermal damage threshold observed in Fig. 5 corresponds to the denaturation of one or more proteins essential to SGN function.

If we relax the requirement for similar laser pulse timescales, some previous studies of INS damage thresholds can then be compared with the present results. Goyal et al. conducted cochlear stimulation experiments *in vivo* at a significantly higher pulse rate than our own (250 Hz for 3 hours) and reported a functional damage threshold of 25-40 μJ per pulse [21]. In this case, the short inter-pulse gap is likely to have contributed to significant cumulative heating [41], leading to

Biomedical Optics EXPRESS

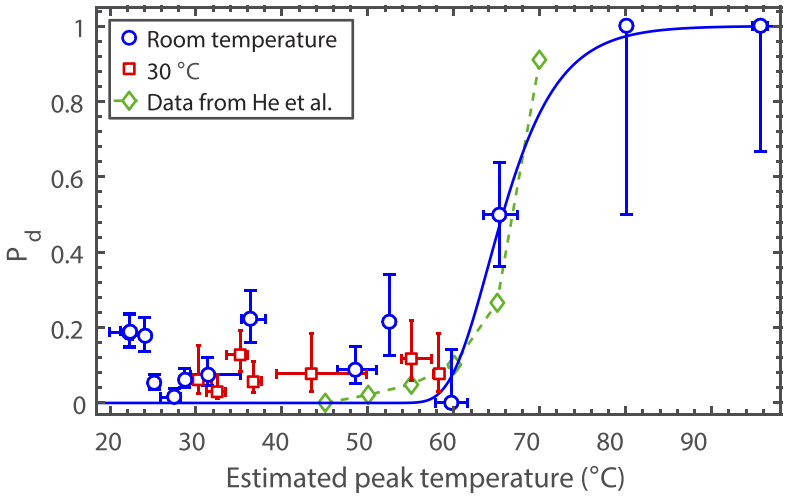

Fig. 5. Thermal threshold for infrared-evoked cell damage. Damage probability is plotted as a function of the estimated maximum temperature exposure per recording, including data from both room temperature and elevated temperature conditions. The solid line is a best-fit MTSH model for the room temperature condition. Data from He and Bischof [39] is included for comparison (see text).

a pulse energy threshold much lower than that observed in Fig. 3(c) (in addition to starting from a 37 °C baseline). Although a direct temperature comparison is difficult to infer, we can calculate the corresponding average laser power as 6.25-10 mW, which lies just below the results reported in Fig. 3(e). In contrast, Chernov et al. histologically identified a damage threshold at around 0.3-0.4 J cm^{-2} in brain tissue (200 Hz for 0.5 s *in vivo*) [17]. For a hypothetical SGN with a typical diameter of 20 μm, this is equivalent to a pulse energy threshold of approximately 0.9-1.3 μJ, and an average pulse power threshold of 0.19-0.25 mW. Similarly, Wells et al. identified a damage threshold for *in vivo* sciatic nerves at 0.66-0.70 J cm^{-2} pulse energy and low repetition frequency [16]. Given that these previously reported studies were conducted *in vivo*, it is perhaps unsurprising that they predict a lower threshold than our results suggest, owing to the pressure of the non-absorbing tissue culture substrate that provides a relatively efficient heat sink. However, the comparison does serve to highlight the difficulties in translating the present result to live animals: although we may still expect the presence of a damage threshold that is dependent on peak temperature, the location of this threshold is likely to be shifted *in vivo*.

4. Conclusion

During infrared stimulation experiments, increases in the energy per pulse, average power and cumulative exposure were found to increase the probability of SGN damage, as defined by a 30% drop in membrane impedance. This implicated peak temperature as the underlying mechanism, for which we identified a threshold at 60 °C. Future work in SGNs should investigate the effects of large pulse energies at higher ambient temperatures, since insufficient data was available above 3 mJ for this study. We also note that this 60 °C threshold is likely to be significantly shifted for *in vivo* studies, due to the differing thermodynamics of *in vitro* and *in vivo* environments. Furthermore, patch clamped cells are in an inherently non-physiological state, and may therefore be more susceptible to thermal damage.

The analysis presented here suggests that damage thresholds can in principle be calculated with some degree of confidence, regardless of the exposure parameters. Since membrane impedance

Biomedical Optics EXPRESS

is always recorded either implicitly or explicitly during patch-clamp recordings, our analysis method can be applied to estimate damage probability from existing data and does not expand recording requirements. Future work should perform a more systematic study of cell damage characteristics in order to confirm the role of peak temperature as the apparent dominant factor, rather than the net change or rate of change in temperature.

Thermal injury is typically characterised by multistate thermodynamic probability models, in particular the Arrhenius injury model [18]. In this study we have elected to keep the MTSH model for Fig. 5 in order to demonstrate the flexibility of the MTSH model for applications where the underlying damage mechanism is not certain. Further studies which seek to clarify the link between peak temperature and thermal damage should consider the implementation of such a model to better characterise hyperthermal damage kinetics.

The MTSH model and Weibull description of cumulative failure probability have been applied in other areas of biology, including cells exposed to ionising radiation [32] and thermal inactivation of bacteria for food sterilisation [42]. However, these techniques should allow the calculation of a wide range of dose-dependent damage thresholds and, to the best of our knowledge, this is the first time that they have been applied to the study of damage thresholds of neurons exposed to laser light. Importantly, this approach is well-suited to quantifying gradual neuronal damage, and threshold behaviour is not required. Therefore the methods described here are likely to be useful for determining the safety of the many less-invasive techniques for neural stimulation that are currently emerging [1,2].

Funding

Australian Research Council Linkage Project (LP120100264).

Disclosures

The authors have nothing to disclose.

References

1. W. L. Hart, T. Kameneva, A. W. Wise, and P. R. Stoddart, "Biological considerations of optical interfaces for neuromodulation," Adv. Opt. Mater. **7**(19), 1900385 (2019).
2. P. M. Lewis, R. H. Thomson, J. V. Rosenfeld, and P. B. Fitzgerald, "Brain Neuromodulation Techniques: A Review," Neuroscientist **22**(4), 406–421 (2016).
3. S. Diemert, A. M. Dolga, S. Tobaben, J. Grohm, S. Pfeifer, E. Oexler, and C. Culmsee, "Impedance measurement for real time detection of neuronal cell death," J. Neurosci. Methods **203**(1), 69–77 (2012).
4. J. Wells, C. Kao, K. Mariappan, J. Albea, E. D. Jansen, P. Konrad, and A. Mahadevan-Jansen, "Optical stimulation of neural tissue in vivo," Opt. Lett. **30**(5), 504 (2005).
5. J. Wells, C. Kao, P. Konrad, T. Milner, J. Kim, A. Mahadevan-Jansen, and E. D. Jansen, "Biophysical mechanisms of transient optical stimulation of peripheral nerve," Biophys. J. **93**(7), 2567–2580 (2007).
6. M. G. Shapiro, K. Homma, S. Villarreal, C.-P. Richter, and F. Bezanilla, "Infrared light excites cells by changing their electrical capacitance," Nat. Commun. **3**(1), 736 (2012).
7. E. S. Albert, J. M. Bec, G. Desmadryl, K. Chekroud, C. Travo, S. Gaboyard, F. Bardin, I. Marc, M. Dumas, G. Lenaers, C. Hamel, A. Muller, and C. Chabbert, "TRPV4 channels mediate the infrared laser-evoked response in sensory neurons," J. Neurophysiol. **107**(12), 3227–3234 (2012).
8. A. D. Izzo, C. P. Richter, E. D. Jansen, and J. T. Walsh, "Laser stimulation of the auditory nerve," Lasers Surg. Med. **38**, 745–753 (2006).
9. J. M. Cayce, R. M. Friedman, G. Chen, E. D. Jansen, A. Mahadevan-Jansen, and A. W. Roe, "Infrared neural stimulation of primary visual cortex in non-human primates," NeuroImage **84**, 181–190 (2014).
10. A. C. Thompson, P. R. Stoddart, and E. D. Jansen, "Optical Stimulation of Neurons," Curr. Mol. Imaging **3**(2), 162–177 (2015).
11. A. R. Duke, M. W. Jenkins, H. Lu, J. M. McManus, H. J. Chiel, and E. D. Jansen, "Transient and selective suppression of neural activity with infrared light," Sci. Rep. **3**(1), 2600 (2013).
12. E. H. Lothet, K. M. Shaw, H. Lu, J. Zhuo, Y. T. Wang, S. Gu, D. B. Stolz, E. D. Jansen, C. C. Horn, H. J. Chiel, and M. W. Jenkins, "Selective inhibition of small-diameter axons using infrared light," Sci. Rep. **7**(1), 3275 (2017).
13. S. Yoo, S. Hong, Y. Choi, J. H. Park, and Y. Nam, "Photothermal inhibition of neural activity with near-infrared-sensitive nanotransducers," ACS Nano **8**(8), 8040–8049 (2014).

Biomedical Optics EXPRESS

14. S. Yoo, R. Kim, J.-H. Park, and Y. Nam, "Electro-optical Neural Platform Integrated with Nanoplasmonic Inhibition Interface," ACS Nano **10**(4), 4274–4281 (2016).
15. M. Plaksin, E. Shapira, E. Kimmel, and S. Shoham, "Thermal Transients Excite Neurons through Universal Intramembrane Mechanoelectrical Effects," Phys. Rev. X **8**(1), 011043 (2018).
16. J. D. Wells, S. Thomsen, P. Whitaker, E. D. Jansen, C. C. Kao, P. E. Konrad, and A. Mahadevan-Jansen, "Optically mediated nerve stimulation: Identification of injury thresholds," Lasers Surg. Med. **39**, 513–526 (2007).
17. M. M. Chernov, G. Chen, and A. W. Roe, "Histological assessment of thermal damage in the brain following infrared neural stimulation," Brain Stimul. **7**(3), 476–482 (2014).
18. R. Liljemalm and T. Nyberg, "Quantification of a thermal damage threshold for astrocytes using infrared laser generated heat gradients," Annals Biomed. Eng. **42**(4), 822–832 (2014).
19. A. D. Izzo, J. T. Walsh, E. D. Jansen, M. Bendett, J. Webb, H. Ralph, and C. P. Richter, "Optical parameter variability in laser nerve stimulation: A study of pulse duration, repetition rate, and wavelength," IEEE Trans. Biomed. Eng. **54**(6), 1108–1114 (2007).
20. S. M. Rajguru, A. I. Matic, A. M. Robinson, A. J. Fishman, L. E. Moreno, A. Bradley, I. Vujanovic, J. Breen, J. D. Wells, M. Bendett, and C. P. Richter, "Optical cochlear implants: Evaluation of surgical approach and laser parameters in cats," Hear. Res. **269**(1-2), 102–111 (2010).
21. V. Goyal, S. Rajguru, A. I. Matic, S. R. Stock, and C. P. Richter, "Acute damage threshold for infrared neural stimulation of the cochlea: Functional and histological evaluation," Anat. Rec. **295**, 1987–1999 (2012).
22. A. I. Matic, A. M. Robinson, H. K. Young, B. Badofsky, S. M. Rajguru, S. Stock, and C. P. Richter, "Behavioral and Electrophysiological Responses Evoked by Chronic Infrared Neural Stimulation of the Cochlea," PLoS One **8**(3), e58189 (2013).
23. W. G. A. Brown, K. Needham, B. A. Nayagam, and P. R. Stoddart, "Whole Cell Patch Clamp for Investigating the Mechanisms of Infrared Neural Stimulation," J. Vis. Exp. **77**, 50444 (2013).
24. A. C. Thompson, S. A. Wade, W. G. A. Brown, and P. R. Stoddart, "Modeling of light absorption in tissue during infrared neural stimulation," J. Biomed. Opt. **17**(7), 0750021 (2012).
25. A. Mansoorifar, A. Koklu, and A. Beskok, "Quantification of cell death using an impedance-based microfluidic device," Anal. Chem. **91**(6), 4140–4148 (2019).
26. K. F. Lei, M. H. Wu, C. W. Hsu, and Y. D. Chen, "Real-time and non-invasive impedimetric monitoring of cell proliferation and chemosensitivity in a perfusion 3D cell culture microfluidic chip," Biosens. Bioelectron. **51**, 16–21 (2014).
27. F. A. Atienzar, H. Gerets, K. Tilmant, G. Toussaint, and S. Dhalluin, "Evaluation of impedance-based label-free technology as a tool for pharmacology and toxicology investigations," Biosensors **3**(1), 132–156 (2013).
28. J. R. Lepock, "Cellular effects of hyperthermia: Relevance to the minimum dose for thermal damage," Int. J. Hyperther. **19**(3), 252–266 (2003).
29. J. Yong, K. Needham, W. G. Brown, B. A. Nayagam, S. L. McArthur, A. Yu, and P. R. Stoddart, "Gold-Nanorod-Assisted Near-Infrared Stimulation of Primary Auditory Neurons," Adv. Healthcare Mater. **3**, 1862–1868 (2014).
30. H. T. Beier, G. P. Tolstykh, J. D. Musick, R. J. Thomas, and B. L. Ibey, "Plasma membrane nanoporation as a possible mechanism behind infrared excitation of cells," J. Neural Eng. **11**(6), 066006 (2014).
31. L. D. Brown, T. T. Cai, and A. DasGupta, "Interval Estimation for a Binomial Proportion," Statist. Sci. **16**(2), 101–133 (2001).
32. J. E. Turner, D. J. Downing, and J. S. Bogard, *Statistical Methods in Radiation Physics* (Wiley-VCH, 2012).
33. J. Yao, B. Liu, and F. Qin, "Rapid temperature jump by infrared diode laser irradiation for patch-clamp studies," Biophys. J. **96**(9), 3611–3619 (2009).
34. J. M. Bec, E. S. Albert, I. Marc, G. Desmadryl, C. Travo, A. Muller, C. Chabbert, F. Bardin, and M. Dumas, "Characteristics of laser stimulation by near infrared pulses of retinal and vestibular primary neurons," Lasers Surg. Med. **44**, 736–745 (2012).
35. R. Liljemalm, T. Nyberg, and H. Von Holst, "Heating during infrared neural stimulation," Lasers Surg. Med. **45**, 469–481 (2013).
36. L. Paris, I. Marc, B. Charlot, M. Dumas, J. Valmier, and F. Bardin, "Millisecond infrared laser pulses depolarize and elicit action potentials on in-vitro dorsal root ganglion neurons," Biomed. Opt. Express **8**(10), 4568 (2017).
37. J. Gallaher, K. Wodzińska, T. Heimburg, and M. Bier, "Ion-channel-like behavior in lipid bilayer membranes at the melting transition," Phys. Rev. E **81**(6), 061925 (2010).
38. A. C. Thompson, S. A. Wade, P. J. Cadusch, W. G. A. Brown, and P. R. Stoddart, "Modeling of the temporal effects of heating during infrared neural stimulation," J. Biomed. Opt. **18**(3), 035004 (2013).
39. X. He and J. C. Bischof, "The kinetics of thermal injury in human renal carcinoma cells," Ann. Biomed. Eng. **33**(4), 502–510 (2005).
40. M. W. Dewhirst, B. L. Viglianti, M. Lora-Michiels, M. Hanson, and P. J. Hoopes, "Basic principles of thermal dosimetry and thermal thresholds for tissue damage from hyperthermia," Int. J. Hyperther. **19**(3), 267–294 (2003).
41. A. C. Thompson, S. A. Wade, N. C. Pawsey, and P. R. Stoddart, "Infrared neural stimulation: Influence of stimulation site spacing and repetition rates on heating," IEEE Trans. Biomed. Eng. **60**(12), 3534–3541 (2013).
42. M. A. J. S. van Boekel, "On the use of the Weibull model to describe thermal inactivation of microbial vegetative cells," Int. J. Food Microbiol. **74**(1-2), 139–159 (2002).